TECHNICAL NOTE

D-1251

STRUCTURAL BEHAVIOR AND COMPRESSIVE STRENGTH OF

CIRCULAR CYLINDERS WITH LONGITUDINAL STIFFENING

By James P. Peterson, Ralph O. Whitley,
and Jerry W. Deaton

Langley Research Center
Langley Station, Hampton, Va.

NATIONAL AERONAUTICS AND SPACE ADMINISTRATION

WASHINGTON   May 1962

NATIONAL AERONAUTICS AND SPACE ADMINISTRATION

TECHNICAL NOTE D-1251

STRUCTURAL BEHAVIOR AND COMPRESSIVE STRENGTH OF

CIRCULAR CYLINDERS WITH LONGITUDINAL STIFFENING

By James P. Peterson, Ralph O. Whitley,
and Jerry W. Deaton

L
1
9
6
1

SUMMARY

Results of compression tests on 17 circular cylinders with longitudinal stiffening are presented and discussed. In addition, supplementary studies of the compressive load-shortening characteristics of plates with large width-thickness ratios and of the strength of columns consisting of longitudinally stiffened sheet which buckled prior to column failure are given and employed in analyses of the cylinder tests. Correlation between experiment and analysis was achieved in predicting local buckling of the skin and in predicting the load-shortening characteristics of the cylinders. Correlation was also achieved in predicting the panel-instability loads of the longer cylinders, but the shorter cylinders failed at loads considerably less than those predicted, evidently by a mode of deformation not considered in the analysis.

INTRODUCTION

The information available on the structural behavior of longitudinally stiffened cylinders in compression is extremely meager; test programs on complete cylinders of proportions representative of those used in aircraft structures and for which structural parameters are systematically varied appear to be completely lacking in the literature. As a consequence, data are needed on all phases of structural behavior including skin buckling and cylinder failure as well as on the deformation characteristics of cylinders under applied load.

The test results reported herein include information on these phases of structural behavior and were obtained on 48-inch-diameter cylinders stiffened longitudinally by Z-section stringers. The structural parameters varied were the width-thickness ratio of the skin panels between stiffeners which had nominal values of 80, 125, and 200 and the length-radius ratio of the cylinders which was varied from 0.7 to 1.4. The tests were conducted on 7075-T6 aluminum-alloy circular

cylinders loaded in compression between the platens of a large testing machine. The results obtained are compared with available theoretical results.

SYMBOLS

A_W	cross-sectional area of stiffener, sq in.
A_{cyl}	cross-sectional area of cylinder, sq in.
b	stiffener spacing, in. (fig. 2)
b_e	effective width of skin between stiffeners, $b \dfrac{\bar{\sigma}}{\sigma_{edge}}$, in.
b_W	depth of web of stiffener, in.
c	coefficient of fixity in Euler column formula
D_1	plate flexural stiffness in longitudinal direction, $\approx \left(EI_x\right)_e$, in-kips
D_2	plate flexural stiffness in circumferential direction, in-kips
D_{xy}	plate twisting stiffness, in-kips
E	Young's modulus, ksi
E_1	plate extensional stiffness in longitudinal direction, kips/in.
E_2	plate extensional stiffness in circumferential direction, kips/in.
E_{sec}	secant modulus of material stress-strain curve, ksi
E_{tan}	tangent modulus of material stress-strain curve, ksi
$\bar{E}_{sec}$	secant modulus of load-shortening curve, ksi
$\bar{E}_{tan}$	tangent modulus of load-shortening curve, ksi

$(EI)_e$ effective bending stiffness of a stiffener-skin assembly, kip-in.^{2}

$(EI_x)_e$ effective longitudinal bending stiffness per inch of circumference of cylinder wall, in-kips

G_{xy} shear stiffness of cylinder wall, kips/in.

I_e effective moment of inertia of a stiffener-skin assembly, in.^{4}

$$\zeta = \frac{b_e}{b} \sqrt{\frac{\bar{\epsilon}}{\epsilon_{cr}}}$$

k, k_∞ buckling coefficient for curved and flat plate, respectively,
$$\frac{12(1 - \mu^2)}{\pi^2} \frac{\sigma_{cr} b^2}{E t^2}$$

l length of cylinder, in.

N_p compressive load per inch of circumference at panel buckling, kips/in.

P column buckling load, kips

R radius of cylinder, in.

t thickness of skin, in.

t_W thickness of stiffener, in.

w_o amplitude of imperfection, in. (ref. 1)

Z curvature parameter, $\dfrac{b^2}{Rt} \sqrt{1 - \mu^2}$

γ empirical correction for initial imperfections (ref. 2)

$\bar{\epsilon}$ unit shortening

ϵ_{cr} computed strain at local buckling of skin, neglecting effect of curvature on buckling

μ Poisson's ratio of skin material

L
1
9
6
1

ρ radius of gyration of cylinder wall about centroidal axis, neglecting local buckling effects, in.

σ_{edge} edge stress corresponding to strain $\bar{\epsilon}$, ksi

$\bar{\sigma}$ average compressive stress due to applied load, ksi

σ_{cr} average compressive stress at local buckling of skin, ksi

$\bar{\sigma}_p$ average compressive stress at panel instability, ksi

$\bar{\sigma}_f$ average compressive stress at failure or maximum load, ksi

Subscripts:

S   skin

W   stiffener

$R = \infty$ radius equal to infinity

PRELIMINARY CONSIDERATIONS

Before proceeding to a discussion of the cylinder tests conducted in this investigation, the results of two supplementary studies which are helpful in interpreting the results of the tests are given. The studies entail an experimental investigation of the stiffness characteristics of flat plates in compression and an analytical investigation of the accuracy of the column formula in predicting the strength of some longitudinally stiffened flat plates which develop skin buckling prior to column failure.

Flat-Plate Tests

Koiter (ref. 3) has conjectured that the advanced postbuckling behavior of a slightly curved plate subjected to axial compression may be similar to that of a geometrically similar but flat plate. His conjecture is depicted graphically for a typical plate in figure 1 where the average stress in the curved plate divided by the buckling stress of the flat plate is plotted against the edge strain (shortening) of the curved plate divided by the buckling strain of the flat plate. Although his conjecture was purposely limited to plates with small

curvature $\left(Z < \dfrac{\pi^2 k_\infty}{2\sqrt{3}}\right)$, figure 1 is constructed without this limitation because, on the basis of the cylinder tests discussed later, his conjecture is believed to have somewhat more general application. Two curves are shown schematically for the curved plate, one representative of a plate without imperfections and one representative of a plate with imperfections.

If, for the moment, figure 1 is assumed to be representative of the behavior of curved plates, and the cylinder tests to be discussed tend to confirm this assumption, it follows that the seemingly difficult task of predicting the postbuckling behavior of curved plates is reduced to that of predicting the load-shortening characteristics of flat plates, a problem which has already received considerable attention. The behavior immediately following buckling is not given by the flat-plate analysis but it is of less practical interest than the advanced buckling stage for many purposes. One difficulty exists in applying flat-plate analyses to curved plates. The width-thickness ratio of curved plates is considerably greater than that of flat plates for which load-shortening analyses have been verified. Hence an experimental study of flat plates with large width-thickness ratios was undertaken. Details of the study are presented in appendix A. The principal results of the study that are useful in the analysis of curved plates are the secant and tangent moduli of the load-shortening curves for flat plates which can be expressed in equation form as follows:

$$\frac{\overline{E}_{sec}}{E_{sec}} = \frac{b_e}{b} = \zeta \sqrt{\frac{\epsilon_{cr}}{\overline{\epsilon}}} \tag{1}$$

and

$$\frac{\overline{E}_{tan}}{E_{sec}} = \left(\frac{E_{tan}}{E_{sec}} - \frac{1}{2}\right)\zeta\sqrt{\frac{\epsilon_{cr}}{\overline{\epsilon}}} + 0.42\left[\left(1 - \sqrt{\frac{\epsilon_{cr}}{\overline{\epsilon}}}\right)\sqrt{\frac{\epsilon_{cr}}{\overline{\epsilon}}}\right]^2 \tag{2}$$

where

$$\zeta = 1 + 0.28\left(1 - \sqrt{\frac{\epsilon_{cr}}{\overline{\epsilon}}}\right)^3$$

Analysis of Column Tests

Because predictions of the strength of longitudinally stiffened curved plates depend to a great extent upon the use of the column formula as applied to stiffened plates that buckle locally at loads

considerably less than the column load, it is desirable to compare predictions made by using the formula with the observed strength of flat panels to determine what errors should be associated with use of the formula when the effects of curvature do not complicate the comparison. Such a comparison has been made with the test data of reference 4 and is presented in appendix B. Results of the comparison indicate that prediction and experiment differ by no more than 10 percent.

CYLINDER TESTS

Tests on 17 circular cylinders stiffened longitudinally with Z-section stringers constituted the principal part of this investigation. The cylinders were approximately 48 inches in diameter (150 inches in circumference) and differed from one another in the width-thickness ratio of the skin between stringers b/t and in cylinder length. Proportions of the cylinders were such that the cylinders experienced skin buckling at rather low loads and buckled into a more general mode at higher loads. The more general mode entailed rather large lateral deformations of the stiffeners and buckled skin as a unit and consisted of several diamond-shape buckles around the circumference of the cylinder. Each buckle encompassed the full length of the cylinder. This type of buckling is hereinafter termed "panel buckling." The tests and some of the results are discussed in this section of the paper.

Test Specimens and Test Procedure

Construction details of the test cylinders are given in figure 2, and some pertinent dimensions of the cylinders are given in table I. The dimensions given are nominal except those given for skin thickness which were obtained by a large number of micrometer measurements and those given for cross-sectional area which were determined by weighing.

The cylinders were fabricated with the with-grain direction of the skin material in the circumferential direction and with a single longitudinal splice in the skin. The stiffeners were attached to the skin with 5/32-inch-diameter spot welds spaced approximately 1/2 inch apart. The circularity of the ends of the cylinders was maintained with the use of 1/4-inch-thick aluminum bulkheads in each end of the cylinders, which had diameters somewhat smaller than the clear distance between diametrically opposed stiffeners. The bulkheads were held in place by a low-temperature ($\approx 160^\circ$ F) potting material. The ends of the cylinders were machined flat and parallel and the cylinders were tested with the bulkheads and potting material in place. The skin splice was made with a double row of spot welds, one row which served also to attach a

stiffener to the skin. In a few cylinders some of these welds failed during the machining operation and were replaced with blind rivets.

The cylinders were constructed of 7075-T6 aluminum alloy. Typical material properties were used in reducing the data. Young's modulus E was taken as 10,500 ksi, Poisson's ratio μ was assumed to be 0.32, and the material density was assumed to be 0.101 pound per cubic inch.

The cylinders were loaded in compression in the Langley 1,200,000-pound-capacity testing machine after they had been carefully alined in the machine to insure uniform bearing between the ends of the specimens and the platens of the testing machine; one of the platens could be tilted to conform to the machined shape of the specimens. Resistance-type wire strain gages were mounted on the skin and stiffeners of the cylinders prior to testing, and strains from the gages were recorded during the test with the use of an automatic strain recorder. Two types of gages were used: gages with a 13/16-inch gage length were used on the skin to detect local buckling and gages with a 6-inch gage length were used on the stiffeners and on the skin near stiffeners to help detect general buckling of the specimens and to indicate stress distribution in the cylinders. Shortening of the distance between the platens of the testing machine was recorded against load during each test with the use of resistance-type wire strain gages mounted on small cantilever beams whose deflection was equal to the shortening of the distance between platens.

L
1
9
6
1

Test Results and Discussion of Results

Load-shortening curves.- Plots of average compressive stress due to applied load against unit shortening are given in figure 3 for all of the test cylinders except cylinder 15; a load-shortening curve was not obtained for this cylinder. The shaded circles denote the load at which panel buckling was observed. These loads coincide in many cases with sharp breaks in the load-shortening curves. Other sharp breaks correspond to changes in mode shape from one with a certain number of waves around the circumference to one with one more or one less wave than previously. The number of circumferential waves in the panel instability mode is noted on figure 3 for those specimens whose test log included that information.

A calculated curve based on equation (1) and the conjecture advanced by Koiter, that the advanced postbuckling behavior of a curved plate is similar to that of a flat plate of like dimensions, is shown also in figure 3 for comparison. The value of ϵ_{cr} used in the calculation was obtained from the flat-plate buckling charts of reference 1. The stiffeners were assumed to be sturdy and to carry a load equal to

$\left(E_{sec}\right)_W \bar{\epsilon} A_W$. Calculation is generally in rather good agreement with experiment, with computed values of shortening being slightly less than measured values for cylinders with a skin width-thickness ratio of 80 and slightly greater than measured values for cylinders with skin width-thickness ratios of 125 and 200.

The main conclusion to be drawn from figure 3 is that Koiter's conjecture appears to be substantiated by the cylinder data in areas where substantiation can be expected. This area encompasses that portion of the curves from some unspecified point somewhat above the local buckling stress up to the panel buckling stress. Substantiation exists for all cylinders including those with skin panels having considerable curvature and thereby an analytical means for evaluating some of the stiffness properties of buckled cylinders is provided. These stiffnesses are required for predicting panel instability or general instability failures.

Local buckling.- Buckling coefficients as determined by test are plotted against the curvature parameter Z in figure 4. The coefficients shown were determined from the load at which the load-shortening curve of the cylinders deviated from the linear portion of the curve with a slope approximately equal to Young's modulus. Generally, this load could be determined rather precisely because the slope of the load-shortening curve changed rather abruptly when the skin buckled. When buckling was more gradual (generally cylinders with $b/t = 80$), the point of buckling was taken as the intersection of two straight lines used to approximate the curve in the vicinity of the buckling load. Buckling loads determined in this manner are generally higher and their scatter is somewhat less than those determined by observation or by the strain-reversal method (ref. 5). However, in the test cylinders the loads obtained by the three methods were generally in close agreement (differing by less than 5 percent) if the data were adequate to obtain buckling loads by the three methods. In a few tests, however, buckling was observed in local areas of the test cylinders at loads as low as 80 percent of those shown in figure 4, possibly a result of loading the cylinders nonuniformly either due to nonuniform machining on the ends of the cylinders or to an inadequate adjustment of the platens of the testing machine prior to testing. The cylinders with appreciably lower observed buckling loads than those in figure 4 are noted in table I.

Also shown in figure 4 is the buckling stress of the cylinders computed according to reference 1 by using two different assumptions for the initial-imperfection parameter w_o^2/Rt. The lower curve was calculated by using $\dfrac{w_o^2}{Rt} = 0.00065$ which is the value used in reference 1 to achieve correlation with the middle of the scatter band of the data

of reference 6 on single-panel specimens with two angle-shaped stiffeners supporting each of the unloaded edges of the curved sheet. Hence, higher buckling stresses were achieved in the present tests than were achieved in the single-panel tests of reference 6. Had the load at which the first buckles were observed been used to construct figure 4, two of the points at $Z \approx 6.5$ would have fallen below the curve represented by $\frac{w_o^2}{Rt} = 0.00065$.

The upper curve on figure 4 was calculated with $\frac{w_o^2}{Rt} = 0$. It represents the classical small-deflection buckling stress of curved plates in compression as given by reference 7 and upon which the equations of reference 1 are based.

Panel buckling.- The average stress at which panel buckling occurred in each of the test cylinders is recorded in table I. The panel buckling load was taken as that load at which the characteristic diamond-shape buckles could first be seen over a large portion of the cylinder circumference. In some tests panel buckling occurred suddenly over the entire circumference of the cylinder and was accompanied by a falling off in testing machine load; in other tests panel buckling developed more gradually and was unaccompanied by any marked departure from the preceding loading history. (See fig. 3.) One of the cylinders in the panel buckling mode is shown in figure 5.

The panel instability load of the test cylinders can be calculated by using reference 2 provided the required bending and extensional stiffnesses are properly modified to account for the skin being buckled at panel instability. The necessary equation can be written as (ref. 2)

$$N_p = \frac{c\pi^2 D_1}{l^2} + \gamma \frac{2}{R} \sqrt{E_1 D_2} \tag{3}$$

where the stiffnesses D_1, D_2, E_1, and E_2 are needed to determine the panel instability load; the stiffness E_2 is implicit in the factor γ. The calculation of $D_1 \approx \left(EI_x\right)_e$ is indicated in the discussion on column tests (appendix B) and the calculation of E_1 follows from the discussion of load-shortening curves for plates (appendix A). The stiffness E_1 was taken as

$$\frac{E_1}{\left(E_{sec}\right)_W t} = \frac{A_W}{bt} + \frac{\left(\overline{E}_{sec}\right)_S}{\left(E_{sec}\right)_W} \tag{4}$$

The stiffnesses D_2 and E_2 were taken rather arbitrarily as

$$\frac{D_2}{E_s t^3} \approx \frac{1}{12} \qquad (5)$$

$$\frac{E_2}{E_s t} = \left(\frac{\bar{E}_{sec}}{E}\right)_s \qquad (6)$$

that is, the bending stiffness in the circumferential direction was
taken as the value for unbuckled sheet and the extensional stiffness of
the buckled skin in the circumferential direction was assumed to be
equal to that of the buckled skin in the axial direction.

Calculations made with the use of equation (3) are given along with
the test data from table I in figure 6. The fixity coefficient c was
taken equal to 3.50, the value used in reference 2 to achieve correla-
tion between cylinder tests and theory, for small applied loads and was
modified for plasticity as in the column calculations of appendix B for
larger applied loads. The calculations with c modified for plasticity
are shown as dashed lines in figure 6. The stress-strain curves employed
were the same as those used in the column calculations, and values for
ϵ_{cr} for the present calculations were obtained in the same manner as
for the column calculations (appendix B). Agreement between calculation
and experiment is reasonably good for the three cylinders in each series
at the higher values of slenderness ratio $l/\rho\sqrt{c}$ and is rather poor for
the two cylinders in each series at the lower values of slenderness
ratio. An explanation for this behavior has not been found. However,
it may be associated with twisting deformations of the stiffeners to
accommodate local buckling of the skin in the advanced local buckling
stage. It was noticed in the course of the tests that the stiffeners
did not provide nodal lines in the advanced local buckling stage; that
is, the local buckles tended to have different circumferential wave
lengths, depending upon whether they were in-buckles or out-buckles.
Because the buckles were alternately in and out around the circumfer-
ence as well as along the cylinder, the stiffener twisted alternately
back and forth along its length to conform with the local buckling pat-
tern of the skin. The twisting increases or decreases the moment of
inertia of the stiffener depending upon the direction the stiffener is
twisted; twisting also induces severe bending stresses in the out-
standing flange of the stiffener which could ultimately cripple the
stiffener and severely reduce its flexural stiffness. The lower panel
buckling loads may be associated with this phenomenon. In order to
determine whether load-induced twisting of stiffeners (as opposed to
buckle-induced twisting as just described) was an important considera-
tion in the failure of the test cylinders, twisting calculations were

made with the use of the equations of reference 8, pages 166 to 171, for flat panels. The calculations indicated that load-induced twisting does not account for the discrepancy between theory and experiment at low values of the slenderness ratio. However buckle-induced twisting which results in crippling of the outstanding flange of the stiffener cannot be discounted on the basis of such calculations.

Of interest also are some calculations that were made to determine the influence of changes in some of the stiffnesses on the calculated panel instability load. Some of the stiffnesses used in the calculations just presented, namely, D_2 and E_2, were chosen arbitrarily and it has been suggested (ref. 8, p. 165) that the stiffness D_2 increases as the skin is loaded from the unbuckled state into the postbuckling range, due to the corrugation effect of the buckles.

The stability equation of reference 9 was used to make the calculations because equation (3) does not apply in this case. In the calculations D_1 and E_1 were taken as before, G_{xy} was conservatively taken as the value given in reference 10 for flat plates, E_2 and D_{xy} were varied in the various calculations made from their estimated value but found to have little influence on the panel instability load, Poisson's ratios for bending and extension were taken as zero, and D_2 was evaluated on the basis of the buckles acting as a corrugated sheet. For the purpose of calculating D_2 the buckle pattern was taken to be sinusoidal in each direction and the buckle depth w was taken as

$$\frac{w}{t} = k_1 \sqrt{\frac{\bar{\epsilon}}{\epsilon_{cr}} - 1} \qquad (7)$$

where the proportionality constant k_1 was taken as unity on the basis of the information given in reference 11 for flat plates. The reduction associated with γ was handled in much the same manner as in equation (3). The resulting panel instability loads were considerably (up to 40 percent) greater than those given in figure 6 for large values of slenderness ratio and slightly (up to 10 percent) greater at small values of slenderness ratio. The increase resulted from the increase in D_2 and not from the use of a different stability equation because the two equations yielded essentially the same buckling loads in separate calculations made by using $\frac{D_2}{Et^3} = \frac{1}{12}$ and values for the other stiffnesses as given previously.

This result suggests that the increase in D_2 associated with local buckling may not exist; but the test for whether it does or does

not exist is admittedly not a good one because of other uncertainties in the calculations. It would seem however that the increase in stiffness from local buckling should not be relied upon in calculations for instability failures of stiffened shells, at least until additional information is available which clears up some of the uncertainties which exist in prescribing values to stiffnesses and in the use of the various stability equations concerned.

Failure.- Most of the test cylinders took some additional load after panel buckling, and some cylinders, generally the longer cylinders with the smaller values of b/t, took an appreciable amount more (table I). Failure of the shorter cylinders was usually accompanied by weld failures and crippling of the stiffeners in areas of severe local bending. (See fig. 7.) Failure of the longer cylinders with $\frac{b}{t} = 200$ were also of this type; however, maximum load for the longer cylinders with $\frac{b}{t} = 125$ and 80 were often characterized by a growth of the panel instability mode and an ultimate falling off in testing-machine load. For some of these cylinders data recording was stopped before a maximum load was reached and for two cylinders (cylinders 3 and 4) loading was stopped before a maximum load was reached in order to save the cylinders for further visual and photographic study. In this regard, the loading history prior to panel instability was considered to be of principal concern. The loading history above the panel instability load was deemed of lesser interest because of the large deformations associated with the high loads.

CONCLUDING REMARKS

Results of compression tests on 17 circular cylinders with longitudinal stiffening are presented and discussed. Attempts at predicting test results are also given. Correlation between experiment and analysis was obtained in the areas of skin buckling and load-shortening behavior and in the area of panel buckling for the longer test cylinders. Correlation was not achieved for panel buckling of the shorter test cylinders whose behavior was evidently influenced by a mode of deformation not considered in the analysis. Additional tests are needed to resolve the discrepancy between theory and experiment in this latter area.

Langley Research Center,
    National Aeronautics and Space Administration,
        Langley Air Force Base, Va., February 13, 1962.

APPENDIX A

COMPRESSIVE TESTS TO DETERMINE POSTBUCKLING BEHAVIOR

OF FLAT PLATES

Test Specimens and Test Procedures

The dimensions of the test specimens used in determining the post-buckling behavior of flat plates are given in figure 8. The specimens were loaded in compression in the Langley 1,200,000-pound-capacity testing machine. The ends of the specimens were machined flat and par-allel prior to testing, and the specimens were carefully alined in the testing machine to insure uniform bearing between the ends of the speci-mens and the platens of the testing machine. Shortening of the distance between the platens of the testing machine was autographically recorded against load during each test with the use of resistance-type wire strain gages mounted on small cantilever beams whose deflection was equal to the shortening of the distance between platens.

Results and Discussion

Results of the tests are shown in figure 9. The curves in the figure were obtained by fitting to the data a curve of the form

$$\frac{b_e}{b} = \zeta \sqrt{\frac{\epsilon_{cr}}{\bar{\epsilon}}} \tag{A1}$$

where the parameter ζ is a function of $\epsilon_{cr}/\bar{\epsilon}$. Equation (A1) was used because previous analytical analyses of the postbuckling behavior of flat plates have indicated that the effective-width ratio can be expressed by an equation of this type.

In figure 10 the test results are also shown plotted against the parameter ζ, along with the results of some selected analytical studies that have been made on the effective width of long flat plates in com-pression. On this type of plot Von Kármán's equation (ref. 12), which is given by equation (A1) with $\zeta = 1.0$, is represented by the horizon-tal line $\zeta = 1.0$. Koiter's results (ref. 13) are given by the upper-most curve on the figure and apply with only small errors to plates having either simply supported or clamped edges as well as to plates having elastically restrained edges in which the restraint is independ-ent of stress and buckle length. The curve showing Stein's results (ref. 11) lies between that of Von Kármán and Koiter and represents one

of the more accurate analyses to date for long simply supported plates
in the postbuckling range immediately following buckling and up to edge
strains of about six times the buckling strain.

Only those test points with tails on the load-shortening curves of
figure 9 were used in figure 10 in obtaining an expression for the effec-
tive width of flat plates. The test points at values of shortening not
much greater than the buckling strain were not used because this region
is the most sensitive to initial imperfections which may exist in the
test specimens (ref. 5) and the points at high values of edge strain
were not used because plasticity effects become important in this range.
However, the good agreement between the test data and the empirical
curves in this latter range (fig. 9) indicates that the plasticity por-
tion of the curves is also adequately predicted for specimens with values
of b/t less than about 125; the data for specimens with larger values
of b/t are not given for loads approaching the crippling load because
failure of these specimens initiated from the sides due to the inability
of the flanges in providing adequate support to the adjacent plates at
the high loads. Hence the failures were not true crippling failures.

This agreement between the test data and the empirical curves at
high loads is somewhat surprising because crippling investigations on
flat plates with width-thickness ratios less than about 60 have shown
that the theoretical load-shortening curve is about 8 percent too high
on the average at maximum (crippling) load (refs. 14 and 15). This dis-
crepancy is probably the result of initial imperfections, which are
known to be important for the low ratios of edge strain to buckling
strain pertinent to plates with small width-thickness ratios, and of
the type of test specimens that have generally been used. Investigations
were generally made on plates supported in V-groove fixtures which may
not support the plate adequately in the advanced postbuckling stage.
The increase in compressive yield stress in the formed corners over that
in the plate, which is appreciable for some materials, is not believed
to be very important. The test specimens made from thin sheets were
formed cold in the as-received condition; the specimens made from thicker
sheets were formed in the as-received condition by heating the areas to
be bent to approximately $200°$ F. Little or no increase in yield strength
is anticipated in either of these operations in view of the fact that
the specimens were made with the cross-grain direction of the material
in the longitudinal direction of the specimens and reference 16 indicates
that little increase in yield stress should be anticipated when loading
is in the cross-grain direction. Further substantiation for the argu-
ment that the formed corners have little effect on the crippling strength
of the test specimens is obtained when one considers that an increase of
say 10 percent in compressive yield stress in the formed corner of a
crippling specimen was found to increase the crippling strength by only
about $2\frac{1}{2}$ percent. (See ref. 14.) This small increase is a result of

the crippling strength of the plate being approximately proportional to the square root of the compressive yield stress and of the crippling strength of plates with formed corners appearing to be about equally dependent upon the yield stress of the plate and the yield stress of the formed corner.

The equation of the curve labeled "empirical" in figure 10 is given by

$$\frac{b_e}{b} = \zeta \sqrt{\frac{\epsilon_{cr}}{\bar{\epsilon}}} \tag{A1}$$

where

$$\zeta = 1 + 0.28 \left(1 - \sqrt{\frac{\epsilon_{cr}}{\bar{\epsilon}}} \right)^3$$

The secant and tangent moduli of the load-shortening curve are sometimes useful. They are given by

$$\bar{E}_{sec} = E_{sec} \left(\frac{b_e}{b} \right) = E_{sec} \zeta \sqrt{\frac{\epsilon_{cr}}{\bar{\epsilon}}} \tag{A2}$$

and

$$\bar{E}_{tan} = \left(E_{tan} - \frac{E_{sec}}{2} \right) \zeta \sqrt{\frac{\epsilon_{cr}}{\bar{\epsilon}}} + 0.42 E_{sec} \left[\left(1 - \sqrt{\frac{\epsilon_{cr}}{\bar{\epsilon}}} \right) \sqrt{\frac{\epsilon_{cr}}{\bar{\epsilon}}} \right]^2 \tag{A3}$$

where E_{sec} and E_{tan} are the secant and tangent moduli of the plate material at a value of strain equal to the edge strain $\bar{\epsilon}$.

APPENDIX B

ANALYSIS OF COLUMN TESTS OF SHEET-STIFFENER PANELS

Determination of the column strength of sheet-stiffener assemblies with the sheet buckled is best accomplished by converting the sheet-stiffener column, which has different properties in the skin and stiffeners by virtue of the skin being buckled to an equivalent column having material properties of the stiffener, and then computing the column load in the usual manner by using the tangent modulus in place of Young's modulus if the column stress is in the plastic range. (See ref. 17.) Conversion of the column may be accomplished by multiplying the skin width b by $\left(\overline{E}_{tan}\right)_S / \left(E_{tan}\right)_W$ where $\left(\overline{E}_{tan}\right)_S$ is the tangent modulus of the load-shortening curve of the skin and $\left(E_{tan}\right)_W$ is the tangent modulus of the stress-strain curve of the stiffener; both moduli are evaluated at a given value of edge strain $\overline{\epsilon}$. The assumption is made here that the stiffener has a sturdy cross section and does not develop local buckling; the skin and stiffener may have different stress-strain curves, however.

The column strength of the sheet-stiffener column is given by

$$P = \frac{c\pi^2 (EI)_e}{\mathit{l}^2} \tag{B1}$$

where $(EI)_e = \left(E_{tan}\right)_W I_e$ and I_e is the effective moment of inertia of the section obtained by converting the column to one having material properties of the stiffener. The load P can be expressed in terms of the edge stress σ_{edge} as

$$P = \sigma_{edge} \left[A_W + bt \frac{\left(\overline{E}_{sec}\right)_S}{\left(E_{sec}\right)_W} \right] \frac{\left(E_{sec}\right)_W}{\left(E_{sec}\right)_S} \tag{B2}$$

where $\left(\overline{E}_{sec}\right)_S$, $\left(E_{sec}\right)_S$, and $\left(E_{sec}\right)_W$ are the respective secant moduli of the load-shortening curve of the skin, the stress-strain curve of the skin, and the stress-strain curve of the stiffener; again the moduli are evaluated at the chosen value of edge strain $\overline{\epsilon}$. Since both sides of equation (B2) depend upon $\overline{\epsilon}$, the process for computing the column load is one of successive approximation. Values of $\left(\overline{\overline{E}}_{sec}\right)_S$ and $\left(\overline{E}_{tan}\right)_S$ are given by equations (A2) and (A3), respectively.

The above equations have been applied to selected panel tests (from ref. 4) and the results are given in figure 11. Only panels with sturdy stiffeners and with large values of width-thickness ratios of the skin were chosen for study. Furthermore, only those panels with the largest ratios of stiffener thickness to skin thickness were chosen; these panels are more representative of the proportions found in longitudinally stiffened curved-sheet construction and their failure is more likely to be representative of failures associated with curved sheet. The compressive stress-strain curves employed in the calculations for figure 11 had pertinent properties which differed little from the average values given in reference 4 for the test panels. Typical stress-strain curves were used which had a value for Young's modulus of 10,500 ksi, a proportional limit of 55 ksi, and 0.2-percent-offset yield stresses of 72 ksi and 78 ksi, respectively, for the skin and stiffeners. The values of ϵ_{cr} used in the calculations were obtained from reference 1.

Preliminary calculations indicated that the computed failing loads were too high for short columns which develop edge stresses in the plastic range. This result probably indicates that the effective column length of a plastic column tested flat-ended between the platens of a testing machine should be considerably greater than that of a similarly tested elastic column for which measurements of effective column length have been made (ref. 18); the plastic column may develop "plastic hinges" near the ends of the column because of the high compressive stresses associated with restraint of bending in these areas. Accordingly, if the applied stress of the column approaches the compressive yield stress, it is inconceivable that any appreciable clamping exists and the effective length should be nearly the actual length as in a simply supported column. The calculations for figure 11 were made therefore with a correction to the fixity coefficient. It was assumed that the fixity coefficient obtained from elastic tests applied up to edge stresses equal to 80 percent of the proportional limit stress, that a coefficient of unity applied above an edge stress of 80 percent of the compressive yield stress, and that the coefficient varied linearly with edge stress between these values. The correction used is arbitrary but a better value cannot be determined from the present data because column load is rather insensitive to fixity coefficient in this range.

The test points at a slenderness ratio of about 65 are of particular interest in the present investigation in that column buckling occurred before the edge stress exceeded the proportional limit stress. Most of the test cylinders reported in the body of the paper fall into this category. The agreement between calculation and experiment in this case is reasonably good; none of the test points differ from the predicted slenderness ratio by more than 10 percent. The calculations were made for panels of nominal dimension and the test points were plotted at values for slenderness ratio corresponding to the nominal value of radius of gyration of the panels.

18

REFERENCES

1. Peterson, James P., and Whitley, Ralph O.: Local Buckling of
   Longitudinally Stiffened Curved Plates. NASA TN D-750, 1961.

2. Peterson, James P., and Dow, Marvin B.: Compression Tests on Cir-
   cular Cylinders Stiffened Longitudinally by Closely Spaced
   Z-Section Stringers. NASA MEMO 2-12-59L, 1959.

3. Koiter, W. T.: Buckling and Post-Buckling Behaviour of a Cylindrical
   Panel Under Axial Compression. Rep. S.476, Nationaal Luchtvaart-
   laboratorium (Amsterdam), May 1956.

4. Hickman, William A., and Dow, Norris F.: Data on the Compressive
   Strength of 75S-T6 Aluminum-Alloy Flat Panels Having Small, Thin,
   Widely Spaced, Longitudinal Extruded Z-Section Stiffeners. NACA
   TN 1978, 1949.

5. Hu, Pai C., Lundquist, Eugene E., and Batdorf, S. B.: Effect of
   Small Deviations From Flatness on Effective Width and Buckling of
   Plates in Compression. NACA TN 1124, 1946.

6. Crate, Harold, and Levin, L. Ross: Data on Buckling Strength of
   Curved Sheet in Compression. NACA WR L-557, 1943. (Formerly
   NACA ARR 3J04.)

7. Stowell, Elbridge Z.: Critical Compressive Stress for Curved Sheet
   Supported Along All Edges and Elastically Restrained Against
   Rotation Along the Unloaded Edges. NACA WR L-691, 1943. (For-
   merly NACA RB 3I07.)

8. Argyris, J. H., and Dunne, P. C.: Part 2. Structural Analysis.
   Structural Principles and Data, Handbook of Aeronautics, No. 1,
   Pitman Pub. Corp. (New York), 1952.

9. Stein, Manuel, and Mayers, J.: Compressive Buckling of Simply
   Supported Curved Plates and Cylinders of Sandwich Construction.
   NACA TN 2601, 1952.

10. Kromm, A., and Marguerre, K.: Behavior of a Plate Strip Under Shear
    and Compressive Stresses Beyond the Buckling Limit. NACA TM 870,
    1938.

11. Stein, Manuel: Loads and Deformations of Buckled Rectangular Plates.
    NASA TR R-40, 1959.

12. Von Kármán, Theodor, Sechler, Ernest E., and Donnell, L. H.:   The
    Strength of Thin Plates in Compression.   A.S.M.E. Trans.,
    APM-54-5, vol. 54, no. 2, Jan. 30, 1932, pp. 53-57.

13. Koiter, W. T.:   De meedragende breedte bij groote overschrijding der
    knikspanning voor verschillende inklemming der plaatranden.   (The
    Effective Width of Flat Plates for Various Longitudinal Edge Con-
    ditions at Loads Far Beyond the Buckling Load.)   Rep. S.287,
    Nationaal Luchtvaartlaboratorium (Amsterdam), Dec. 1943.

14. Anderson, Melvin S.:   Compressive Crippling of Structural Sections.
    NACA TN 3553, 1956.

15. Anderson, Roger A., and Anderson, Melvin S.:   Correlation of
    Crippling Strength of Plate Structures With Material Properties.
    NACA TN 3600, 1956.

16. Woods, Walter, and Heimerl, George J.:   Effect of Brake Forming in
    Various Tempers on the Strength of Alclad 75S-T Aluminum-Alloy
    Sheet.   NACA TN 1162, 1947.

17. Stowell, Elbridge Z.:   A Unified Theory of Plastic Buckling of
    Columns and Plates.   NACA Rep. 898, 1948.   (Supersedes NACA
    TN 1556.)

18. Schuette, Evan H., and Roy, J. Albert: The Determination of Effec-
    tive Column Length From Strain Measurements.   NACA WR L-198, 1944.
    (Formerly NACA ARR L4F24.)

L
1
9
5
1

TABLE I

DIMENSIONS AND TEST RESULTS OF CYLINDERS

Cylinder	l, in.	b, in.	t, in.	A_W, in.^{2}	A_{cyl}, in.^{2}	σ_{cr}, ksi (a)	$\bar{\sigma}_p$, ksi	$\bar{\sigma}_f$, ksi
1	17.0	2.00	0.0249	0.0387	6.65	9.6	27.4	28.1
2	20.0	----	.0244	.0373	6.47	9.7	22.9	23.9
3	25.0	----	.0246	.0375	6.51	9.7	18.1	b19.2
4	30.0	----	.0248	.0382	6.60	10.0	13.0	b15.3
4a	30.0	----	.0248	.0393	6.69	10.0 (8.8)	13.4	18.4
5	34.0	2.00	.0246	.0371	6.48	10.3 (8.3)	11.7	16.8
6	17.0	$3\frac{1}{8}$	.0248	.0388	5.60	4.8	22.4	22.4
7	20.0	----	.0256	.0371	5.64	5.1	17.5	17.9
8	25.0	----	.0256	.0377	5.67	5.4 (4.3)	14.6	15.0
9	30.0	----	.0240	.0382	5.44	5.2	11.4	12.1
10	34.0	$3\frac{1}{8}$	.0247	.0374	5.51	5.4 (4.6)	8.95	10.5
11	17.0	5.00	.0247	.0387	4.88	4.1	15.7	15.9
12	20.0	----	.0248	.0370	4.83	4.3	13.4	13.4
13	25.0	----	.0244	.0370	4.79	4.1	10.8	11.0
14	30.0	----	.0237	.0382	4.72	3.5 (3.0)	8.80	9.52
14a	30.0	----	.0258	.0404	5.09	4.3 (3.6)	9.50	9.75
15	34.0	5.00	.0247	.0374	4.84	c4.4	8.55	8.93

[a]Determined from load-shortening curve. Values in parentheses were determined from direct observation or from strain-gage data and denote buckling which encompassed only small area of cylinder wall.

[b]Greatest applied stress; loading was stopped before maximum load was reached.

[c]Observed buckling stress; no record obtained.
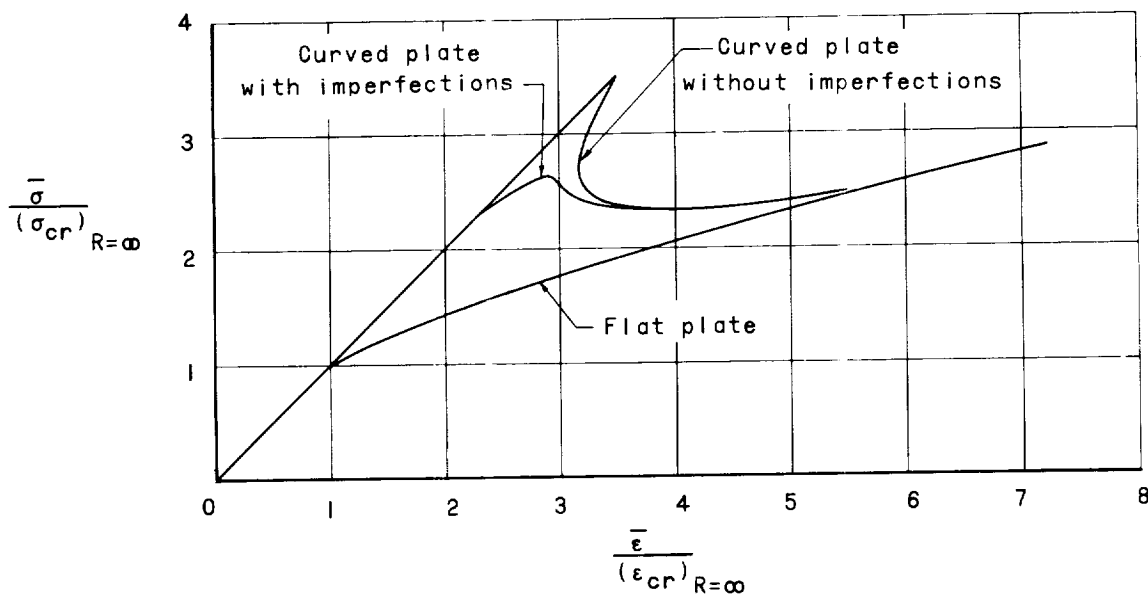
Figure 1.- Schematic representation of load-shortening curves for flat and curved plates.
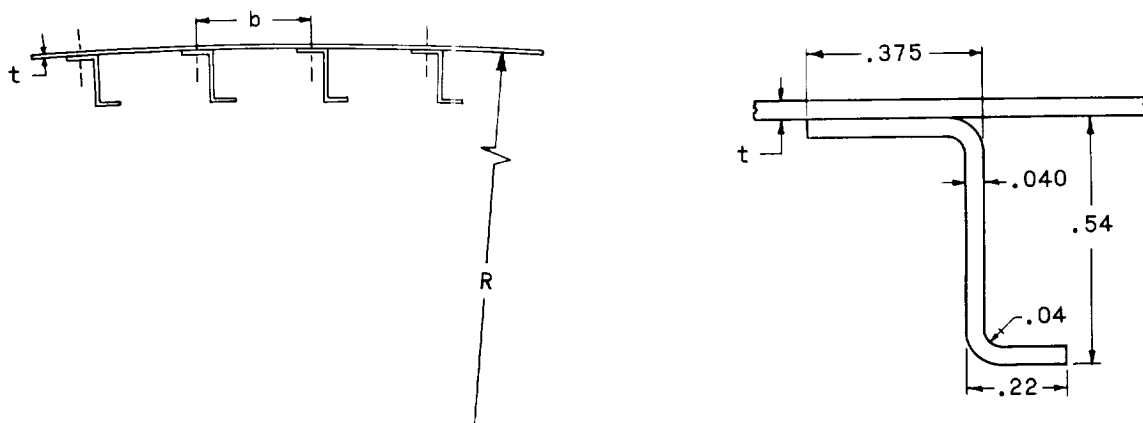
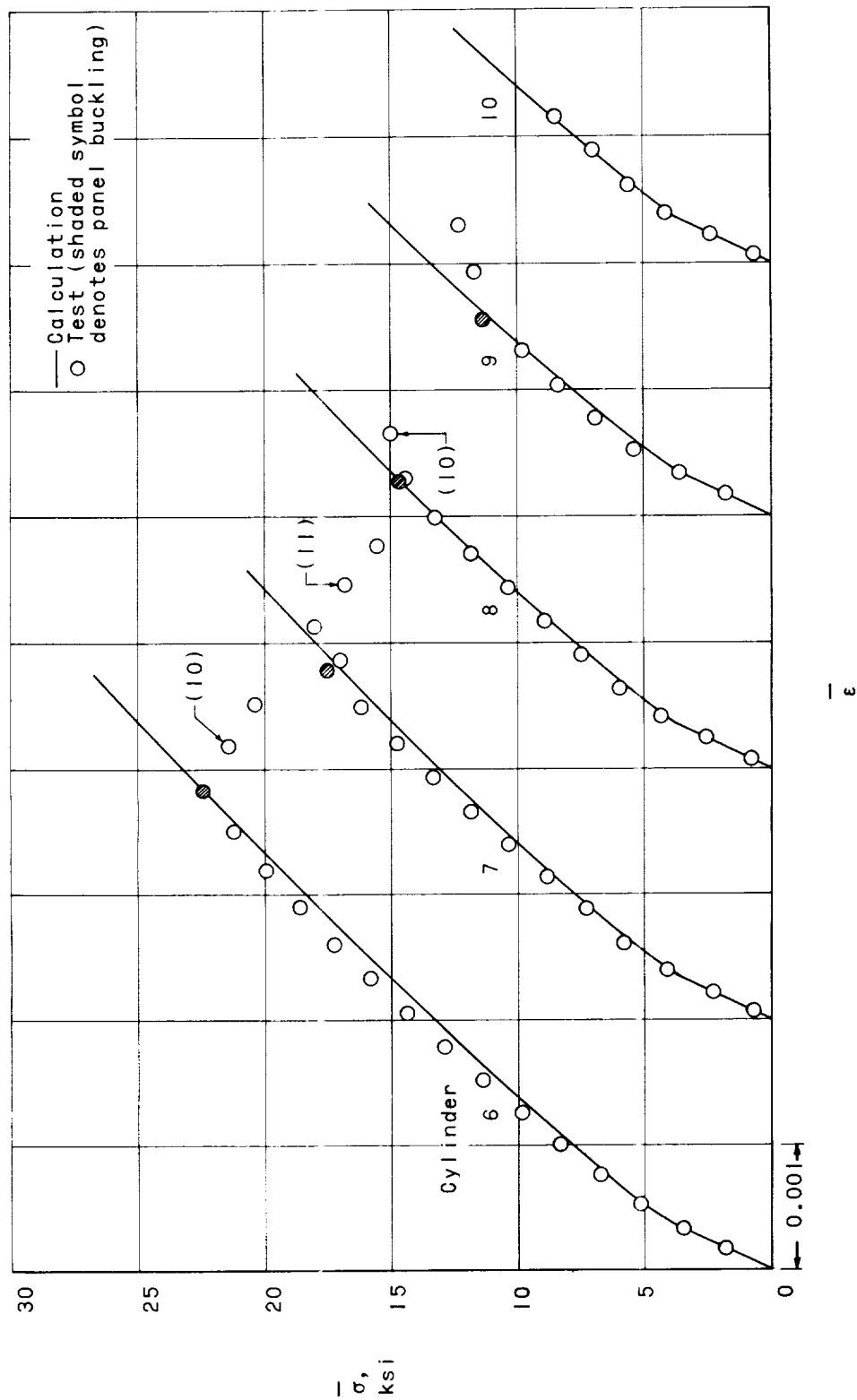(a) Wall details ($2\pi R = 150$ in.).

(b) Stiffener details.

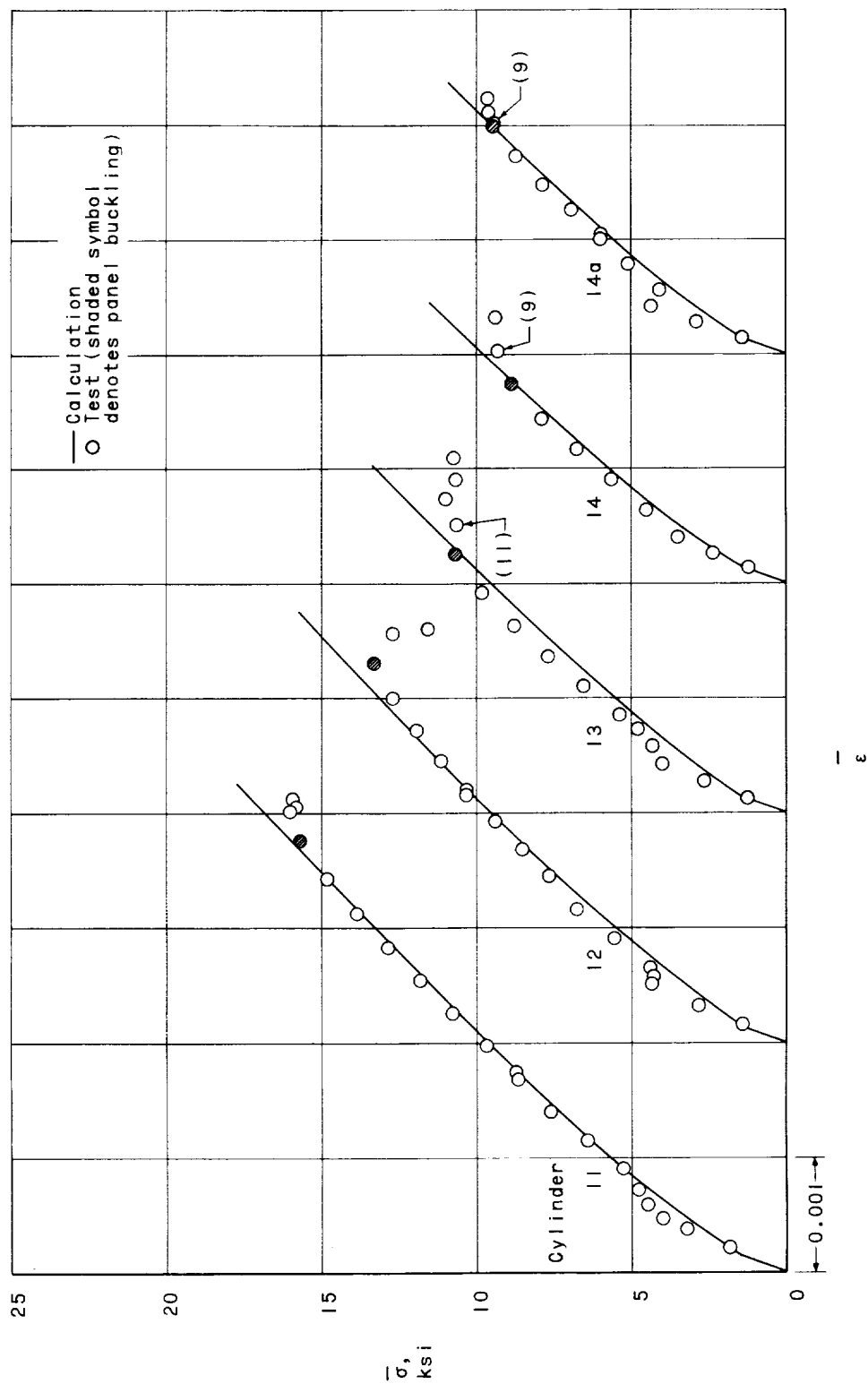Figure 2.- Construction details of test cylinders.
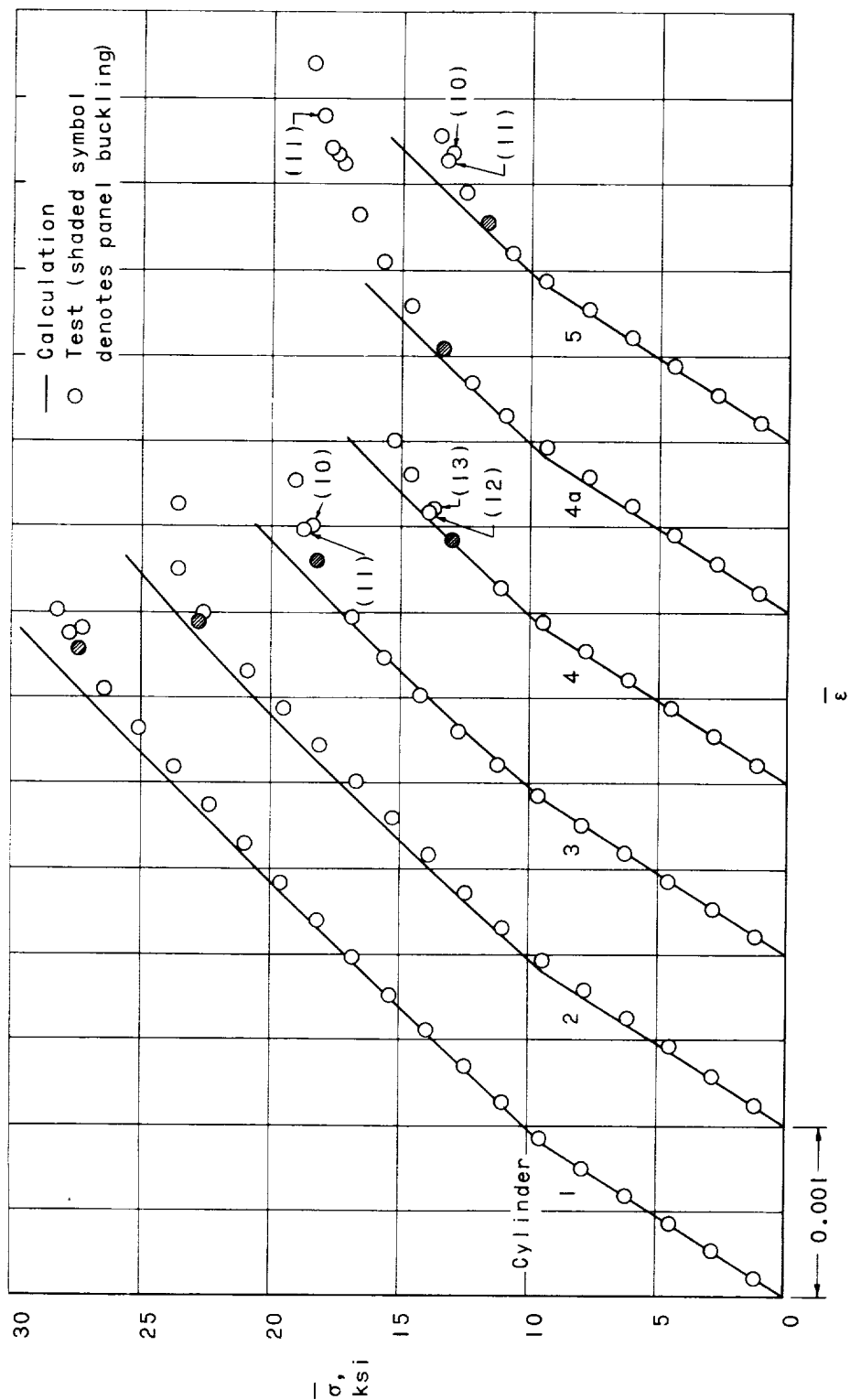
(a) $\frac{b}{t} = 80$.

Figure 3.- Load-shortening curves for test cylinders. Numbers in parentheses denote number of circumferential waves in buckle pattern.

L-1961

(b) $\frac{b}{t} = 125$.

Figure 3.- Continued.
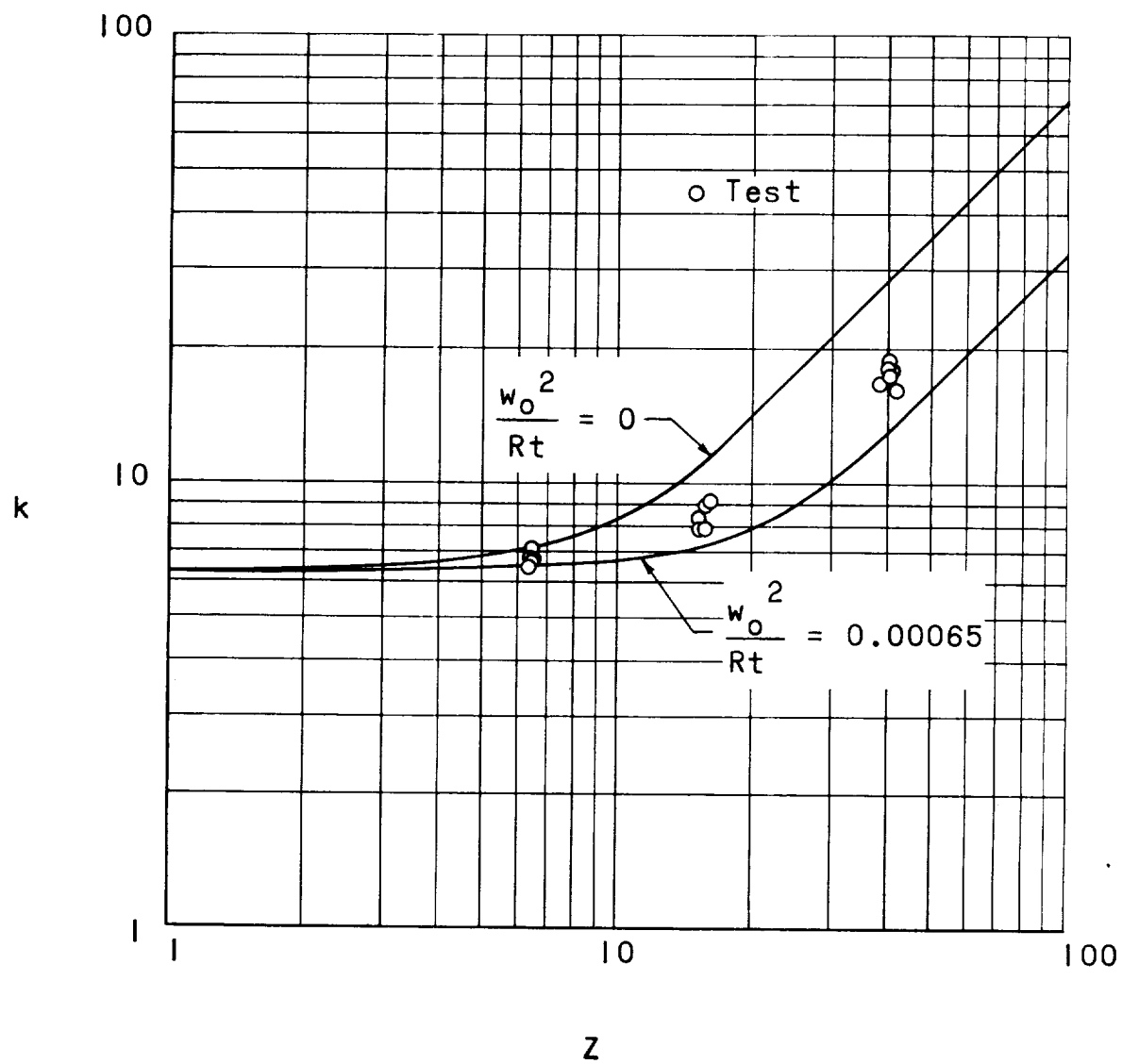
(c) $\frac{b}{t} = 200.$

Figure 3.- Concluded.

Figure 4.- Local buckling of cylinder wall between stiffeners.
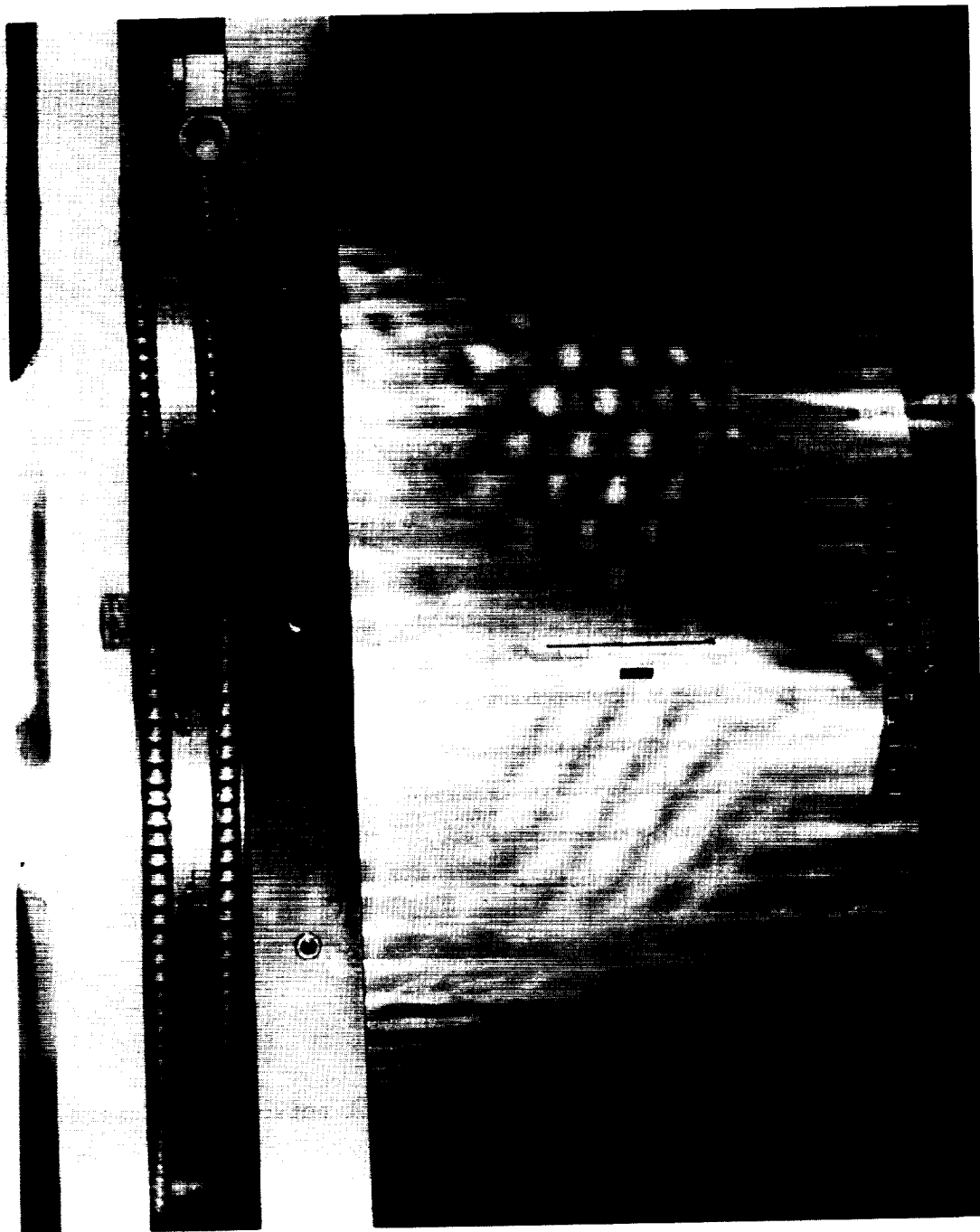
L-60-317

L-1961

Figure 5.- Panel buckling of cylinder 3.

L-1961
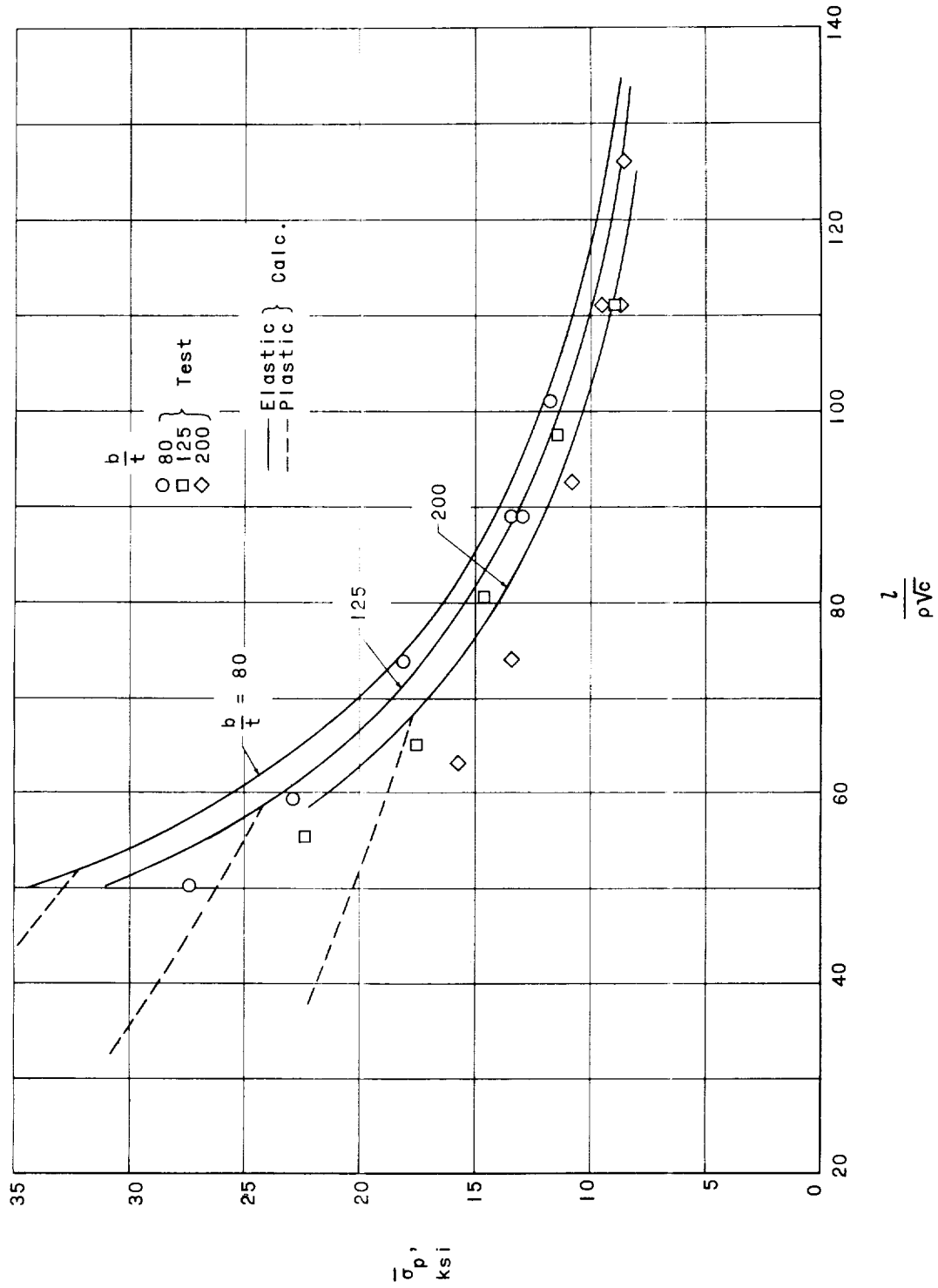
Figure 6.- Panel buckling of test cylinders.

L-61-700

(a) Cylinder 1.

Figure 7.- Failure of short cylinders.

1961

Cylinder II.

L-61-930.1

L-1961

(b) Cylinder 11.

Figure 7.- Concluded.
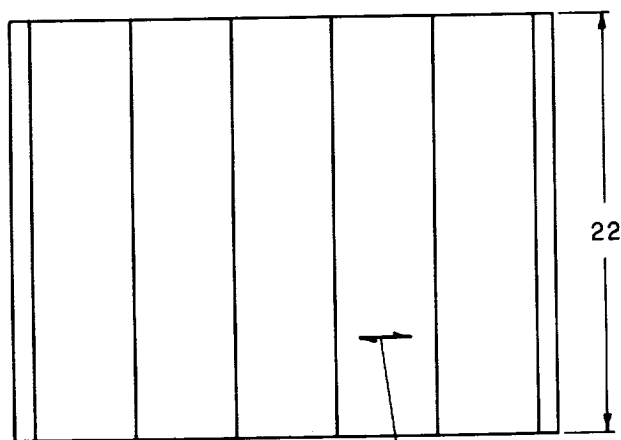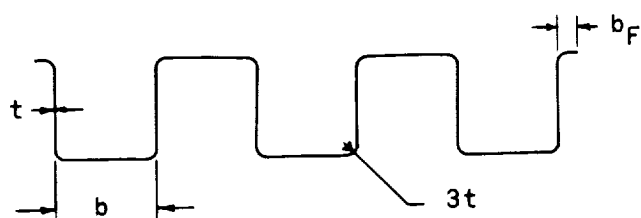
Spec-imen	$\dfrac{b}{t}$	$\dfrac{b_F}{t}$
1a	50.2	0.40
1b	49.7	0.40
2a	77.7	0.40
2b	77.4	0.40
3a	123	0.40
3b	123	0.40
4a	200	0.30
4b	194	0.30
5a	287	0.25
5b	294	0.20

With—grain direction of 7075—T6 aluminum—alloy sheet

Figure 8.- Flat-plate specimens. (b = 5 in., nominally.)
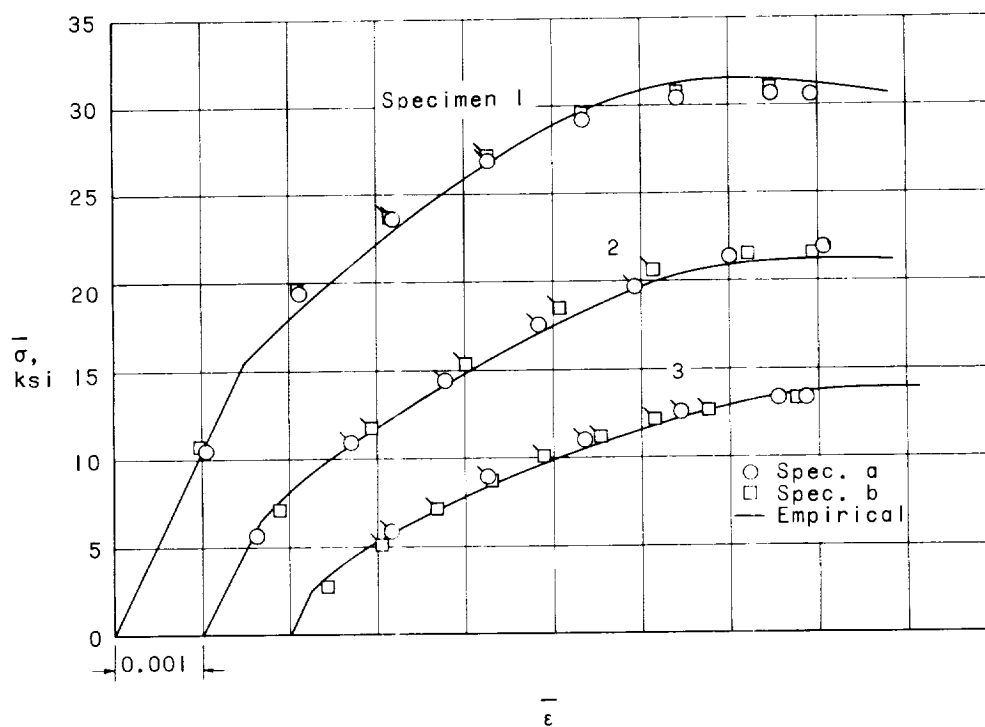
(a) Specimens 1, 2, and 3.
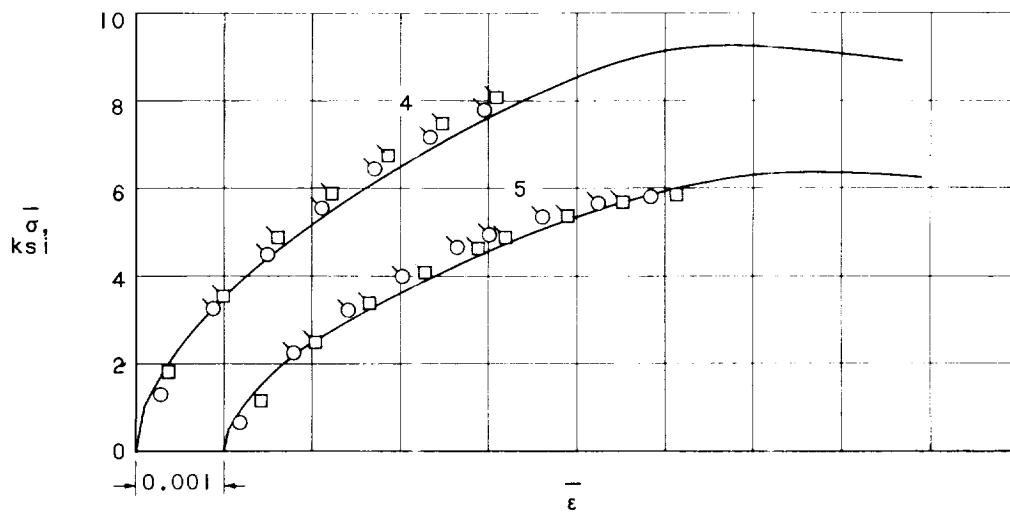
(b) Specimens 4 and 5.

Figure 9.- Load-shortening curves of flat-plate specimens.   Symbols with tails are plotted in figure 10.
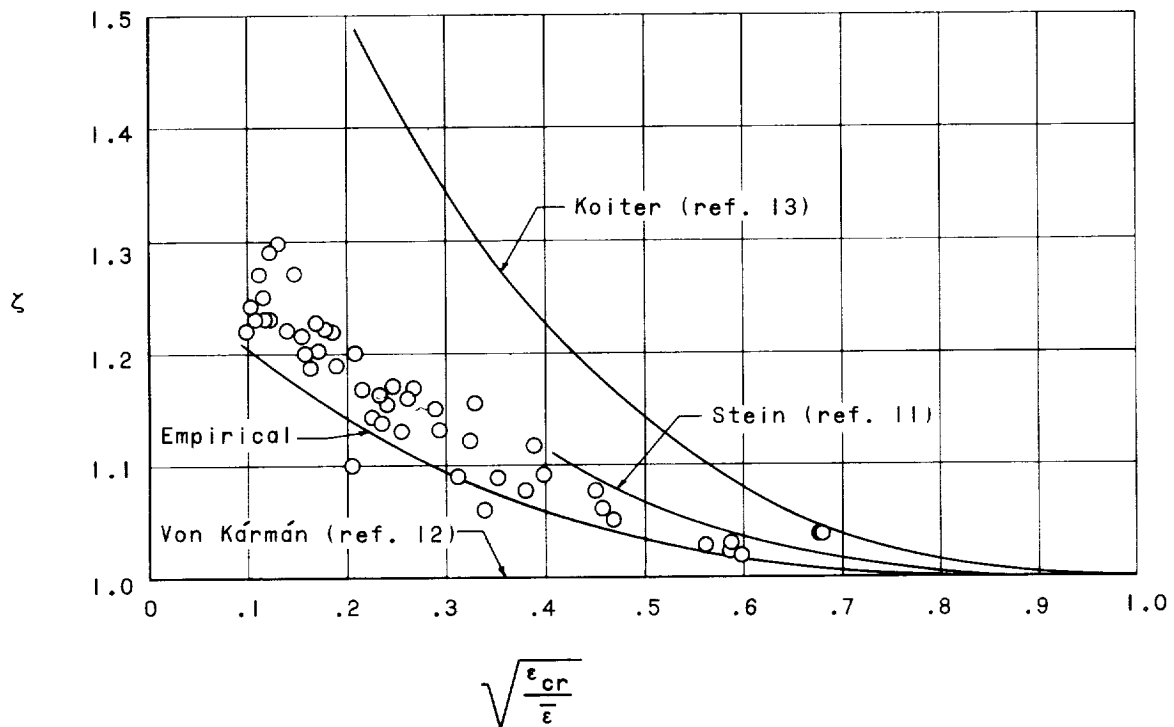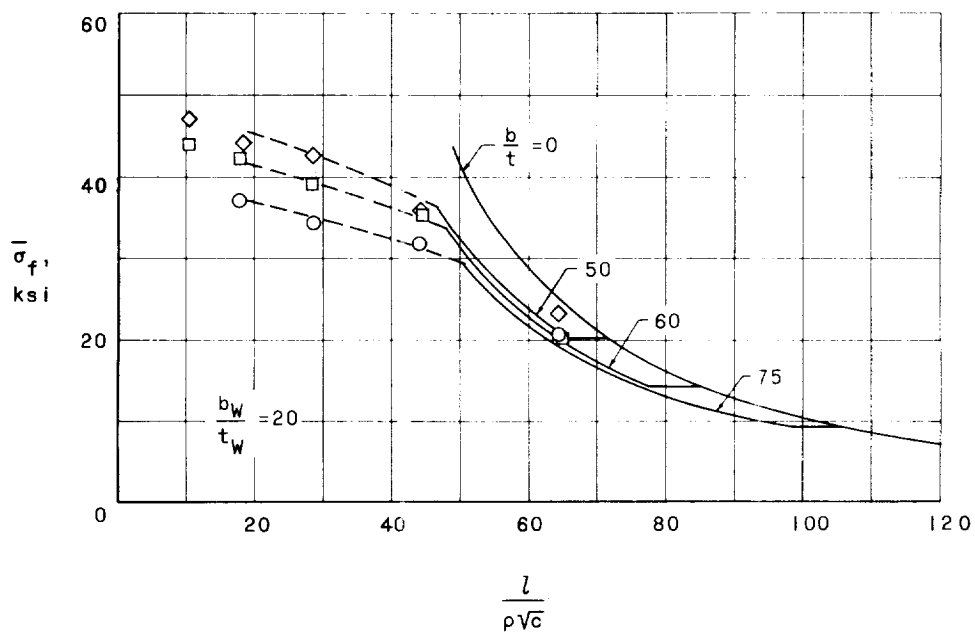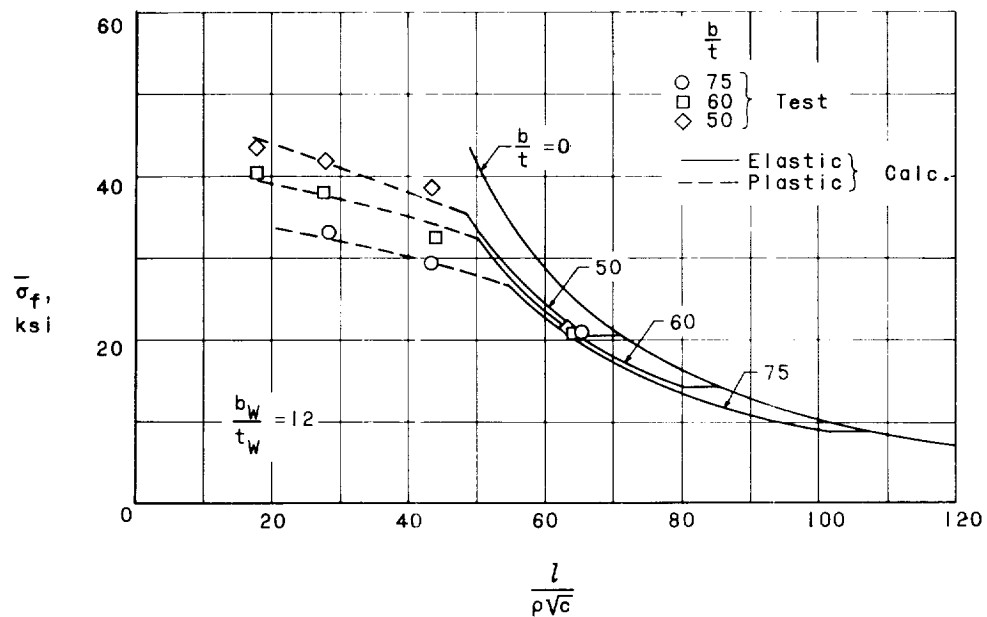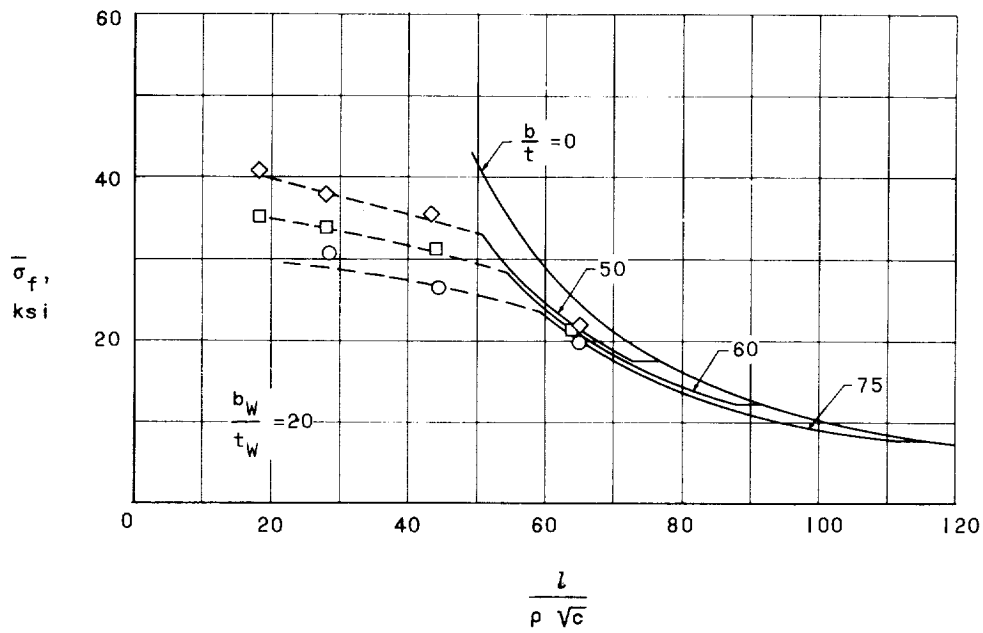
Figure 10.- Comparison of some analytical studies on effective width
of flat plates with test data.

L-1961

Graph 1 (upper):

60

$\frac{b}{t}$

○ 75
□ 60 } Test
◇ 50

$\frac{b}{t}$ = 0

——— Elastic } Calc.
- - - Plastic }

$\bar{\sigma}_f$, ksi

50

60

75

40

20

$\frac{b_W}{t_W}$ = 12

0   20   40   60   80   100   120

$\frac{l}{\rho\sqrt{c}}$

Graph 2 (lower):

60

$\frac{b}{t}$ = 0

$\bar{\sigma}_f$, ksi

50

60

75

40

20

$\frac{b_W}{t_W}$ = 20

0   20   40   60   80   100   120

$\frac{l}{\rho\sqrt{c}}$

(a) $\dfrac{t_W}{t} = 1.00.$

Figure 11.- Comparison between calculation and experiment for panels of reference 4. Only panels with $l > 2b$ are considered.
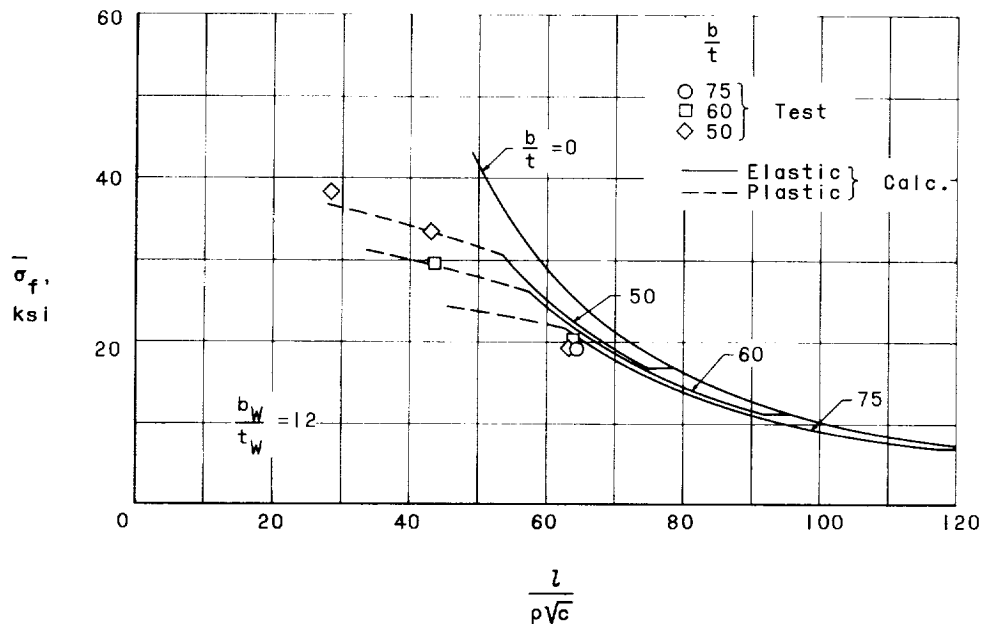
(b) $\dfrac{t_W}{t} = 0.63$.

Figure 11.- Concluded.